Nonequilibrium biochemical structures in two space dimensions with local activation and regulation

B. Fourcade [*]

Grenoble-Alpes University, CNRS, LIPHy, 38000, Grenoble, France

Integrin receptor (IR) clustering is an example of pattern self-organization in biological systems. This paper describes a model for receptor activation whose content is guided by two major principles in cellular signal transduction: (i) Proteins cycle between different conformational states; (ii) the dynamics of their conformational dynamics is environment dependent. Based on a simple activation pathway where these two hypotheses are formulated in a self-consistent way, this paper focuses mainly on stochastic simulations valid in the limit of a small number of molecules. It is shown that coherent clustering can lead to digital signaling and receptor competition in biochemical systems where the model gives a recruitment mechanism for the reinforcement of the mechanical linkage with the extracellular matrix. Together with previous works, this paper provides a workable model for cell integrin adhesive structures when feedback mediated by membrane diffusing signals is dominant. Consequences are discussed in the framework of published data concerning the local production of a key phospholipid for cell signaling (PIP_2).

I. INTRODUCTION

One of the most striking and ubiquitous phenomena in biology is the emergence of self-induced and self-sustained structures. These spatial and temporal structures are archetypes of pattern formation whose self-organization principles are only partly understood [1–5]. In particular, adhesive complexes for cells on substrate grow from nascent adhesions formed of integrin receptors (IR) with no apparent elasticity and develop into more rigid structures connected to the cytoskeleton. Other adhesive structures, called podosomes [6], are characteristic of invasive cells and form a dynamic bestiary of shapes including mesoscopic rings. One ubiquitous property of these structures is the recruitment of IRs into high-density organized clusters to serve as a hub and to process information [7]. The formation of IR-rich clusters having crucial effects on biological responses, it is relevant to study generic mechanisms for their formation.

To study the early stage of IR clustering, the present paper concentrates on a feedback mechanism with a membrane diffusive signal. Since nascent adhesions use adhesome components independently of mechanical forces [8], this paper focuses on signaling properties for receptor clustering using a reaction network where pattern formation is only due to reaction-diffusion processes. Models for clustering such as the purely mechanical trapping of Refs. [9,10] or other general models for signaling components, including lipid rafts and cytoskeleton linkages, have pointed out the role of feedback in spatial clustering of molecules for efficient digital signaling [11] and cell polarization mechanisms [12]. In these works, positive feedback is generally associated with a molecule

promoting its own production and it has been shown that this mechanism leads nanoclusters of active molecules [13,14].

Changes in membrane composition play, however, a key role in IR clustering [15]. It is therefore natural to study how a diffusive membrane signal triggers the emergence of self-sustained IR structures with size comparable to its diffusion length when this signal is locally produced at adhesive sites. In this paper, such a diffusive signal plays the role of an activator and the model mimics key properties of phosphoinositide signaling on IR regulation. In particular, phosphoinositides such as $PtdIns(4,5)P_2$, i.e., PIP_2, are known to regulate actin polymerization factors [16,17] and the membrane cytosol interface by recruiting signaling components [15,18] which, in turn, activate IRs [19–21]. In particular, super-resolutive microscopies [22,23] have shown that a large fraction of IRs are mobile within adhesive clusters with different types of IRs exhibiting distinct dynamics and different spatial organizations [24,25] in a constantly redistributed environment [25].

In the classical continuum framework for a diffusion-reaction model, Ref. [26] has already shown that local production of an activator is enough to cluster IRs. This raises the question whether this model is still valid and what are the different phases in a regime where the number of molecules is small and where the intrinsic noise due to diffusion and reaction dominates.

To this is end, a more general pathway is introduced model appropriate to stochastic simulations which can be generalized to model more mature adhesive structures. As before, the model is guided by two principles in signal transduction: IRs cycle between active and inactive state and the rate of this cycling depends on membrane composition which is determined in a self-consistent way. This model reproduces the sequence of phases (homogeneous, localized spikes, expanding incomplete or complete rings) for different excitation

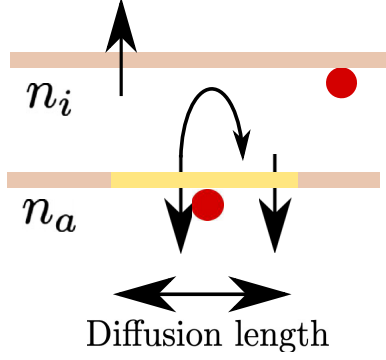———————
[*]Bertrand.Fourcade@univ-grenoble-alpes.fr

012420-1

FIG. 1. Schematic representation of the three modules studied in this paper. Arrows correspond to IRs in their inactive/active-immobile states (n_i, n_a). A change in color in the bar code indicates a local change in composition u within the membrane corresponding to lipid production, i.e., PIP$_2$. An increase of u makes active IRs more stable and, for this reason, u is an activator. The loop arrow represents the local production of the activator u which serves as a positive feedback loop to recruit new receptors in their active state. Regulation of lipid production is controlled by a third field v (red dots) when IRs are immobile. This field v mimics the recruitment of specific kinases such as PIPKIγ to adhesive sites.

levels. The main difference between the stochastic and the deterministic approach is the absence of the self-replicating spot instability with the presence of expanding incomplete arcs in a circle reminiscent of podosome mesostructures. The use of stochastic framework is also appropriate when local production of the activator induces crosstalks and phase segregation for a mixture of receptors competing for immobilization sites. In particular, this paper establishes a casual link between the dynamics of receptors and how one type of receptor can regulate the activation state of a different one [27,28]. As a result, the IRs with the highest residence time are favored and this differential recruitment mechanism predicts a reinforcement for the force transmission through adhesive structures as in other models which rely on a signal to increase IR concentration, see Refs. [29,30] and references therein.

The biological significance of theses results is discussed in the conclusion where this work is put into its biological context with a summary of published data concerning PIP$_2$ signaling and IR clustering. To facilitate the reading, analytical results concerning the conditions under which self-sustained structures exist are reported in the Appendices. Movies from the stochastic simulations are provided as Supplemental Material [31].

II. CONTINUUM MODEL FOR RECEPTOR CLUSTERING

Following Ref. [26], the model is divided into three elementary modules; see Fig. 1 together with Refs. [15,18–20] for their biological significance. The first is a change in membrane composition where $u(\mathbf{x}, t)$ serves as a switch for IR activation. This module simulates local changes in lipid concentration (PIP$_2$) to recruit cytosolic IR activators such as Talin. For this reason, $u(x, t)$ is an activator. Second, IRs are represented with a two-state density field, $[n_i(\mathbf{x}, t), n_a(\mathbf{x}, t)]$. Receptors switch between their inactive and active states with

rates $\omega_\pm(u)$, and an increase in u makes the active state stable. Inactive receptors are free to diffuse, but active ones are immobile, because of their strong affinity to external ligands. In cells, the kinetics of PIP$_2$ synthesis and hydrolysis determines when and where a PIP$_2$ regulated protein can be activated and local production of PIP$_2$ by the lipid kinase PIPKiγ serves to recruit new proteins. For this reason, a third field $v(\mathbf{x}, t)$ is introduced for the local production of $u(\mathbf{x}, t)$. This rate of production of $u(\mathbf{x}, t)$ is proportional to the product of the local density of receptors by $v(\mathbf{x}, t)$, i.e., $v(\mathbf{x}, t)n_a(u)$. Since the depletion of $v(\mathbf{x}, t)$ decreases the production of $u(\mathbf{x}, t)$, this field is a regulator.

In the continuum limit, the pair (u, v) obeys the general equations of motion:

$$\partial_t u = d_u \Delta u + \frac{1}{\varepsilon}[-bu + vn_a(u)],$$

$$\partial_t v = d_v \Delta v + h(v_c - v) - f(v)n_a(u), \quad (1)$$

where d_u, d_v are diffusion constants and b/ε is a rate constant for the irreversible degradation of u. The last term in the second equation, $f(v)n_a(u)$, couples the dynamics of v to the concentration u and $h(v_c - v)$ simulates the exchange of v between the membrane and the cytosol. The function $f(v)$ is general. Since a cluster of receptors indicates a high density of u, and thus a small density of v, we can Taylor expand $f(v)$ for small v as $f(v) = a_0 + a_1 v + \dots$, $a_1 \geqslant 0$.

To complete the system, the equation of motion for (n_i, n_a) follows from the kinetics

$$\partial_t n_i = d_n \Delta n_i - \omega_+(u)n_i + \omega_-(u)n_a,$$

$$\partial_t n_a = +\omega_+(u)n_i - \omega_-(u)n_a, \quad (2)$$

where d_n is the diffusion constant of inactive IRs. Finally, the coupling between the kinetic rates $\omega_\pm(u)$ and the environment $u(x, t)$ is introduced if $u(x, t)$ is interpreted as a chemical potential with

$$\omega_-(u)/\omega_+(u) = \omega_-^0/\omega_+^0 e^{-\beta u}, \quad (3)$$

where β is a positive constant and $\omega_-^0/\omega_+^0 \gg 1$ so that the inactive state is favorable in the low u limit and switches to the active state in the other limit. This sets a lower bound for the characteristic excitation in the spike as

$$u_c = \frac{1}{\beta} \ln \frac{\omega_-^0}{\omega_+^0}. \quad (4)$$

In the model considered here, however, all active IRs are immobilized to external ligands, and $1/\omega_-(u)$ should be interpreted as a residence time which is typically much longer than a conformational interconversion rates [32]. The chemical potential difference between the two conformations should also depend logarithmically on the cytosolic concentration of an activator protein, but this log-dependence is subdominant with respect to the linear dependence in u. For simplicity, this term will be neglected. However, since u serves as docking sites for large proteins such as Talin which regulate IR activation, the effective diffusion of u is affected and is less than for a usual lipid. This work assumes, therefore, that components have almost equal diffusion constants, $d_u \simeq d_v \simeq d_n$.

As shown in the inset of Fig. 2, the problem defined by Eq. (1) together with Eq. (2) has a unique fixed point (u_h, v_h)
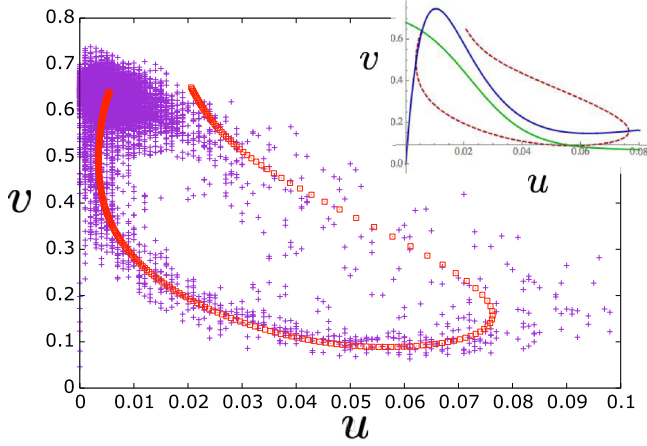
FIG. 2. Nullclines and trajectories $[v(t), u(t)]$ for Eq. (1) in the limit of constant receptor density. The inset shows a typical trajectory when the system is perturbed away of its homogeneous fixed point (u_h, v_h) where the two blue and red curves intersect. The main figure represents the same time trace trajectory for the equivalent problem but in the stochastic limit with the emergence of a stochastic limit cycle absent in the deterministic case. This limit is studied in Sec. III with a reference receptor density per compartment of 1000.

at low u for a broad range of parameters. Neglecting diffusion, the shape of typical trajectories in the (u, v) plane demonstrates that this system is excitable because of the following reason. All initial conditions within a small neighborhood of a stable fixed point give trajectories that decay directly to it, but some initial conditions further away from the stable fixed point give trajectories that undergo large excursions before approaching the fixed point. These excursions are controlled by the parameter ε in Eq. (1), so that when ε is small, large excursions are expected.

Following a δ-like initial perturbation, numerical integration of the time-dependent equations of motion Eqs. (1) + (2) converges to localized static or dynamic self-sustained structures as in Fig. 3. These structures exist only in some regions of the parameter space where the system is excitable enough [26] and a typical phase diagram is shown in Fig. 4. As studied in Appendix A, these structures are localized due to local production of the activator u with clusters of active IRs on a scale comparable to the diffusion length $l_u = \sqrt{d_u \varepsilon / b}$. The other length scale characterizing the problem is set by the diffusion length of the activator, $l_v = \sqrt{d_v / \tilde{h}}$, where $\tilde{h}$ differs little from h. As shown in Appendix A, the characteristic scale for the activator in the spike is set by the ratio $d_v v_h / (d_u \varepsilon)$ with logarithmic corrections. To compensate for the consumption of v within the spike, the recruitment of v by lateral diffusion must be strong enough. This sets a condition on the diffusion constant of the regulator v and comparing with Eq. (4) gives $d_v / d_u > \varepsilon u_c / v_h$ as a lower bound. Because of these strong logarithmic corrections present even for $l_v \approx 10 l_u$, this asymptotic criterion gives only trends when compared with numerical data, but this analysis has the advantage of identifying key relevant parameters.

Static solutions such as the spikes or the rings of Fig. 3 correspond to a regime where diffusion and reaction are uncoupled. Receptors can diffuse rapidly through IR
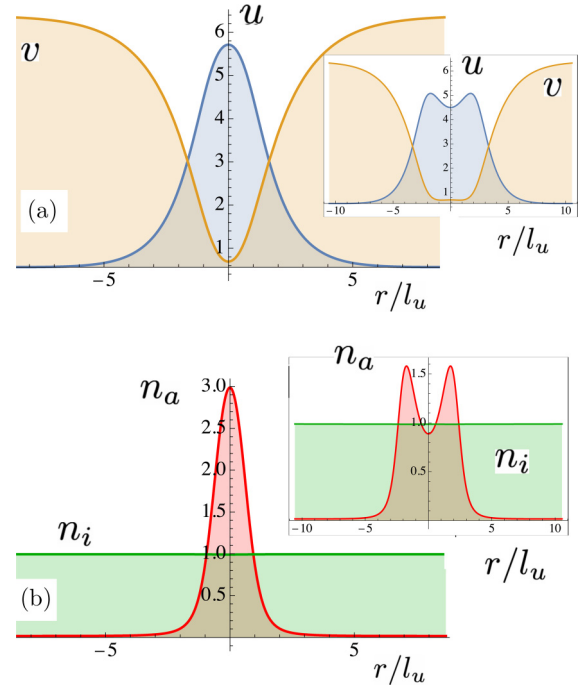

FIG. 3. Plots of stable spike solutions with axial symmetry of rotation. Case (a) corresponds to the activator u in blue and the regulator v in orange. The figure corresponds to a spike solution on the right boundary line of Fig. 4 ($\varepsilon = 5.91$, $d_v = d_u = 1$). The insets show the solution for parameters on the ring boundary line ($\varepsilon = 4$, $d_v = d_u = 1$). Subfigure (b) represents the variations for the inactive (green) and for the active integrin receptors for the same values of the parameters. Note that the density of inactive IRs has converged to one following an initial δ-like perturbation. Going from the spike to the ring solution can be realized by varying the excitability parameter ε or the kinetic rate for membrane recruitment h.

cluster before being immobilized so that IR concentration can be considerably increased. This regime imposes, therefore, a maximum size for the cluster and this criterion is consistent with experimental observations that IRs enter and exit focal adhesions with a significant fraction of mobile IRs [22,33].

III. STOCHASTIC SIMULATIONS

A. A molecular model

For stochastic simulations, it is useful to consider a prototypical molecular pathway of Fig. 5. This biochemical network can be reduced to the model we have considered so far, but this form allows us to point out a key irreversible step in the signaling pathway. To distinguish with the continuum limit, concentrations are represented with capital letters. As before, we assume that all active IRs are immobile and neglect in a first stage any change in free ligand concentration.

A protein V binds an immobilized receptor and undergoes an irreversible post-translational modification which affects its binding to the complex $I_a - V$. The modified form $\varnothing$ is inactive for the production of U and loses its anchor site to the membrane. The down-regulation of the active form of V can also be accomplished through competition for binding
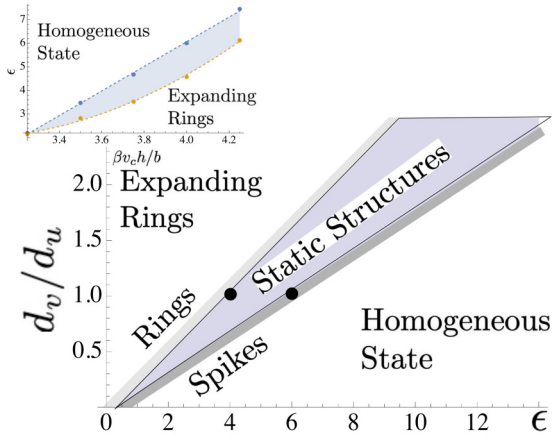
FIG. 4. Schematic phase diagram of the problem Eq. (1). The *x* and *y* coordinates represent the excitability parameter and the ratio of the diffusion constants for the activator *u* and the regulator *v*. For a given ratio hv_c/b, the phase plane is separated into three different regions. At low excitability (large ε), on the right part of the figure, the system returns to the quiescent homogeneous state following a δ-like excitation. Crossing the boundary lines gives static excited solutions. The shape of these solutions are either spikes on the right-hand side of the gray domain or rings on the left; see Fig. 3. For small ratios d_v/d_u, expanding rings are only transient solutions for other sets of parameters. The inset shows the same phase diagram but in the $(hv_c/b, \varepsilon)$ plane for equal diffusion constants $d_v/d_u = 1$. Increasing the flux hv_c makes the system to bifurcate from static to the expanding rings (adapted from Ref. [26], $h = 0.1$, $b = 0.2$, $\beta = 1$, $\omega_-^0/\omega_+^0 = 100$). The two dots correspond to the parameters of Fig. 3 with $(u_h, v_h) \approx (0.56, 6.4)$.

by other cytoskeletal proteins and we define the dwell time τ whose typical order of magnitude corresponds to a few phosphorylation-dephosphorylation cycles. During this dwell time, the complex $I_a - V$ produces U at a rate g_{prod}. In this picture, the depletion of V occurs in tandem with an accumulation of $I_a - V$. V must, however, be continuously fed into the system because of the irreversible step

$$I_a - V \xrightarrow{[1/\tau]} I_a + \varnothing. \quad (5)$$
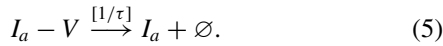
The model can easily generalized by introducing a series $(I_a - V)_i$ of intermediate states before this irreversible step without any changes. As before, the dynamics of U is written
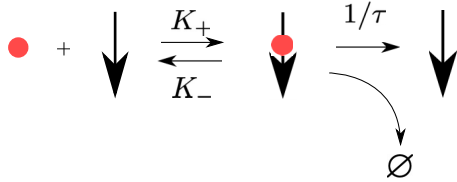

FIG. 5. Schematic pathway considered in the stochastic section. The molecule V (red dot) binds to an immobilized integrin receptor I_a (down arrow) to form a complex $I_a - V$. A covalent modification of V alters the affinity of V to I_a, $V \to \varnothing$. As a consequence, $\varnothing$ unbinds from I_a after a characteristic binding time τ where it loses its anchor site to the membrane.

TABLE I. Correspondence between the stochastic molecular model and the deterministic framework, see Eqs. (1). $K_\pm$ are the binding-unbinding rates of the regulator V to the receptor I. Typical values corresponding to Fig. 6 are $K_+ = 0.01$, $K_- = 1.0$, $H = 0.005$, $V_c = 7.5$, $g_{\text{prod}} = 0.25$, $\beta U = 10U$.

PDE	Stochastic
k_+	$N_0 K_+$
k_-	K_-
$1/\varepsilon$	$g_{\text{prod}} \tau$
b/ε	$(1 + k_- \tau)/k_+ B$
v_c	V_c/N_0
h	$(1 + k_- \tau)/k_+ H$

with the source term proportional to the concentration $I_a - V$,

$$\frac{\partial U}{\partial t} = D_u \Delta U - BU + g_{\text{prod}} I_a - V. \quad (6)$$

In the compartment based approach taken here, the diffusion constants are appropriately renormalized as discussed later. Let $K_\pm$ be the binding and unbinding rates of V to I_a. Since τ is the typical time for a post-translational modification and $1/K_-$ is the binding time for a biochemical bond, we expect $1/\tau \ll K_-$. Assuming that the concentration of the complex $I_a - V$ can be approximated by its pseudo-equilibrium value [34], we have

$$I_a - V = \frac{K_+}{K_- + 1/\tau} I_a \times V, \quad (7)$$

so that the equation for the dynamics of V is

$$\frac{\partial V}{\partial t} = D_v \Delta V + H(V_c - V) - \frac{1}{\tau} I_a - V. \quad (8)$$

Equations (6) and (8) correspond the deterministic model studied so far. The quasiequilibrium Eq. (7) approximation simplifies the problem but will be relaxed in the numerical simulation.

To proceed, it is convenient to scale the number of molecules in compartment *i*, U_i, by reference with the averaged number of receptors N_0 per compartment. The number of molecules in a compartment *i* and the densities are related by

$$\frac{U}{N_0} = \frac{u}{n_0}. \quad (9)$$

The deterministic binding rate is thus related to binding rate per compartment as $k_+ = N_0 K_+$ for $d[I_a - V]/dt = K_+ I_a V$ to be equivalent to $d[n_a - v]/dt = k_+ n_a v$. Table I summarizes the correspondence between the parameters for the stochastic molecular model with their deterministic PDE counterparts, so that the nullclines of Fig. 2 can be compared in the two cases.

After appropriate rescaling, Eqs. (8) and (6) are therefore equivalent to Eq. (1) with an effective dimensionless parameter
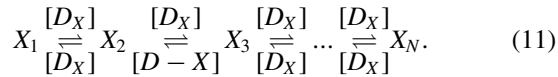
$$\frac{1}{\varepsilon} = g_{\text{prod}} \tau. \quad (10)$$

The value of the molecular model is, therefore, to give a physical meaning of the dimensionless parameter ε as the

ratio of two well-known regulators in cell signaling, i.e., kinase activity and lifetime for a the activation of a molecular architecture.

To complete this reaction scheme, we consider the occupancy probabilities for N discrete compartments of a finite lattice. Let $(I_i, I_a, U, V, I_a-V)_i$ be the number of molecules in compartment i. Our method is standard and we follow Refs. [35,36]. Each compartment is considered homogenous and compartments are coupled via diffusion. An event is either a chemical reaction taking place in a compartment or a stochastic jump from one compartment to its neighbors. The Gillespie's algorithm samples the joint probability distribution for occupancy by simulating the distribution rate for each event and choose the next event to take place [35]. A conformational change of a receptor in a compartment i is considered as an event and the rates $\omega_{\pm}(U_i)$ in compartment i depend on the number of activator molecules U_i in the same compartment. As before, active receptors are assumed to be bound to a ligand and are immobile.

Diffusion is described by the following chain of reactions between nearest neighbor compartments for any specie X_i:

$$X_1 \underset{[D_X]}{\overset{[D_X]}{\rightleftharpoons}} X_2 \underset{[D-X]}{\overset{[D_X]}{\rightleftharpoons}} X_3 \underset{[D_X]}{\overset{[D_X]}{\rightleftharpoons}} \dots \underset{[D_X]}{\overset{[D_X]}{\rightleftharpoons}} X_N. \tag{11}$$

The effective diffusion constant D_X is scaled by the cell size l,

$$D_X = d_x/l^2, \tag{12}$$

where d_x is the usual diffusion constant when the model is written with surface fraction x as in Eq. (1). The definition of the size l is arbitrary. It is convenient to define l as approximately half the size of the diffusion length of u which is the smallest length scale entering in the problem

$$l = 1/2l_u = \tfrac{1}{2}\sqrt{d_u\varepsilon/b}, \tag{13}$$

so that D_u can be directly computed and all other diffusion constants appropriately renormalized. For all the results detailed below, the diffusion constants of the different species are comparable and we use a single compartment size to avoid undesirable bias [36,37]. Using the correspondences of Table I, Fig. 2 compares the phase space trajectories of Eq. (1) in both its stochastic and deterministic versions. Since the stochastic version does not assume stationary equilibrium for the complex I_a-V, Fig. 2 is the projection on the $u-v$ plane of the actual trajectory. Although the traces in two figures appear analogous, the smallness of the number of particles triggers a self-induced stochastic resonance with the apparition of a stochastic limit cycle absent without noise [38]. The appearance of this limit cycle obtained for $N_0 \sim 1000$ molecules is, however, considerably degraded for a smaller number, e.g., ~ 10, where the time series of $u(t)$ exhibits strong bursts emerging from a very noisy signal presenting irregular sequences; see Fig. 6.

As a last point, we discuss how appropriate boundary conditions are implemented with solutions matching their homogeneous fixed point value U_h, V_h, N_0 at infinity. For this, we simulate a probabilistic thermostat in contact with the boundaries. Since molecules outside the simulation box are assumed to diffuse freely, the joint probability to find U_i, V_i or I_i particles in compartment i along the boundaries is a
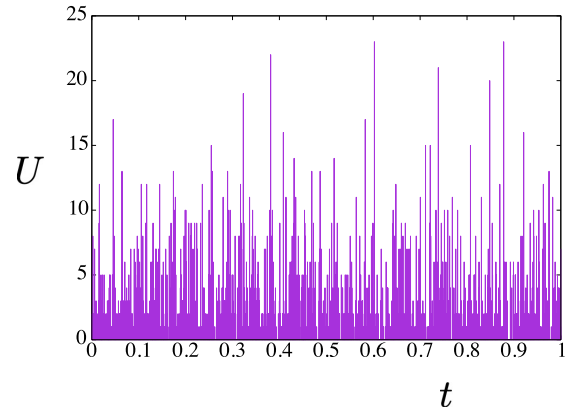

FIG. 6. Single cell stochastic simulation: Number of U molecules as a function of time in the case of a single compartment (homogeneous case). The average number of free integrin receptors per compartment is $N_0 = 10$. This simulation shows that the stochastic dynamics of the activator u exhibits strong irregular bursts above the homogeneous fixed point value ($\langle u \rangle = 0.41$, $\langle v \rangle = 3.91$) given by the deterministic case.

multinomial distribution given by their mean values U_h, V_h or N_0. From a practical point of view, a periodic update of the compartments along the edges by drawing the number of particles according to this distribution simulates this probabilistic Andersen thermostat. Systems from 50×50 to 100×100 compartments can be simulated at a reasonable computing time.

B. Results in the stochastic case

The main results of this section are summarized by the density plots of Fig. 7 for different runs along a line parallel to the ε-axis of Fig. 4 with their corresponding movies in the Supplemental Material [31]. When diffusion is taken into account, stochastic fluctuations are not able to excite the system enough and the homogenous state is characterized by bursts of active receptors with transient small clusters. Receptor clustering is only induced by a threshold perturbation. Following a δ-like excitation with a few tenths of $I_a - V$ molecules in the compartment at the center of simulating domain, one obtains series of snapshots representative of the difference phases. As expected, when the excitability is small, i.e., for ε sufficiently large, a δ-like excitation slowly fades away and the system returns to the homogenous phase. Receptor clustering characterized by a pattern of high density of active receptors occurs only at large enough excitability. When the average number N_0 of receptors is large, i.e., of the order of 100, the static spike of the deterministic framework is reproduced. For lower N_0, i.e., a few 10 the static spike experiences strong breathing deformations and exhibits an intermittent depletion hole in the middle, see case (a), indicating local segregation between the receptors. Even for this relatively large number of molecules, fluctuations are huge and the dynamics processes via bursts. Case (b) of the same figure shows a static spike where the $I - V$ complexes form a ring at the rim of the spike with active receptors centered in the spike (see Supplemental Material for movies [31]). This gradient reflects the strong turnover of V molecules which diffuse from the outside of
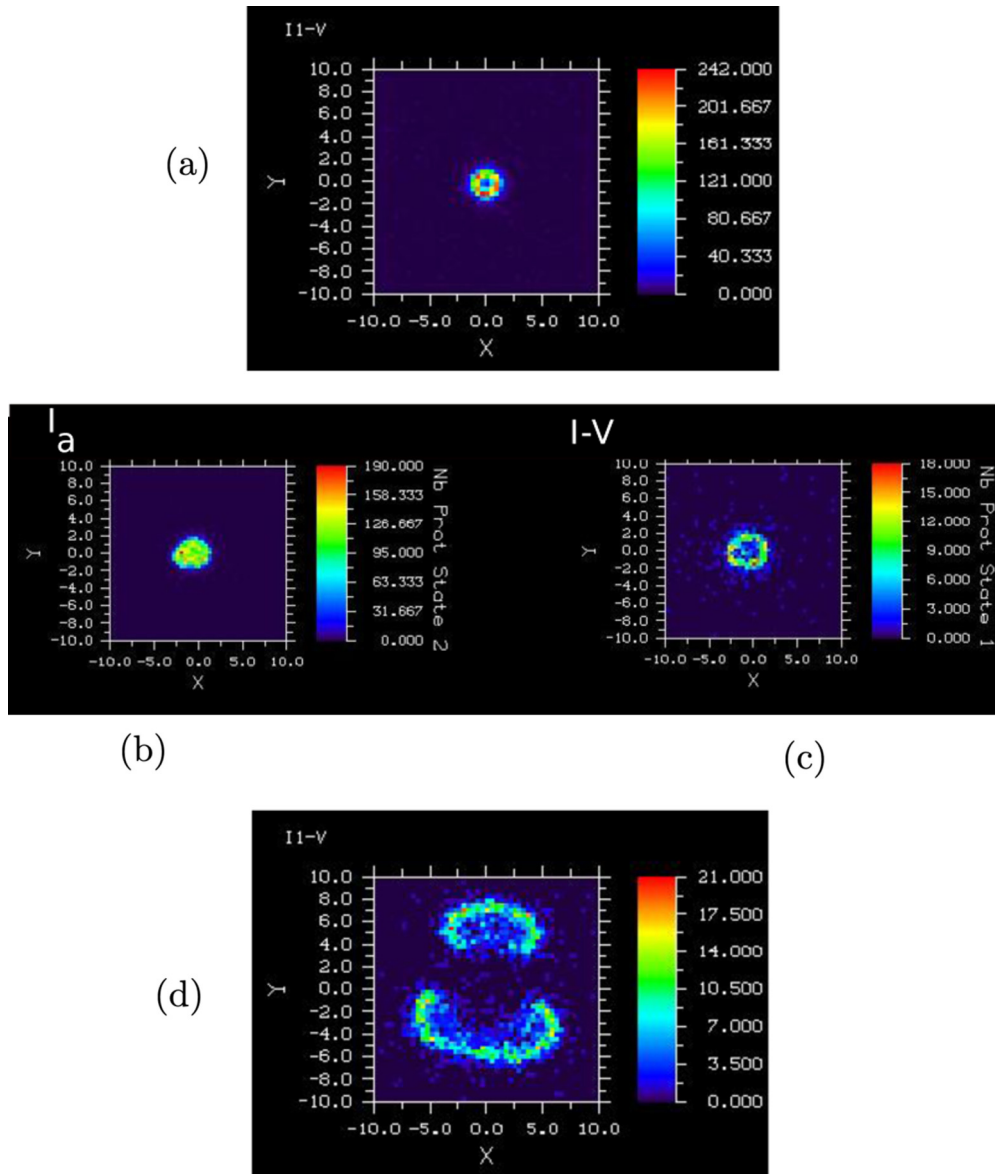
FIG. 7. Examples of density plot for stochastic self-sustained structures taken from snapshots of numerical calculations. Case (a) represents a static spike with a reference number of IRs N_0 equal 100. Immobile-active receptors I_a and complexes $I - V$ are roughly equally distributed with a slight increase of $I - V$ at the rim. For all other cases, $N_0 = 10$. Case (b) is the snapshot of a static spike where the $I - V$ molecules form a fluctuating ring at the rim of the spike. Panel (b) corresponds to active receptors I_a and tpanel (c) to the complex $I - V$. $I - V$ complexes are distributed at the rim of the adhesive spike. Case (d) is the snapshot of an expanding complete ring which becomes incomplete above a critical radius with spiraling ends. Typical parameter values corresponding to (b) are: $\omega_+(0) = 0.001$, $\omega_-(0) = 1$, $HV_c = 2$, $H = 0.05$, $K_+ = 0.1$, $K_- = 1$, $\tau = 1$, $g_{prod} = 3.8$, $B = 0.1425$. For companion movies, see the Supplemental Material [31].

the spike and leave active integrins I_a in the center of the spike. Complete expanding rings are observed in the large excitation regime. In the medium excitation regime, but still in the dynamic part of the phase diagram, complete expanding rings break into circular arcs above a critical radius and form "croissants" with spiraling ends. The size of this critical radius is controlled by the parameters and can be bigger than the simulating box.

In marked contrast with its deterministic counterpart approach, the self-replicating phase has not been observed in numerical simulations. In such phase which appears above a critical radius of an expanding ring, spot-like localized

structures grow, deform and make replicas of themselves until they occupy the entire space. Within the stochastic framework, this phase is replaced by a phenomenon where an expending ring eventually breaks into two or more slowly expanding croissants repealing each other. These structures reach the boundary of the simulating box without further dividing even if the size is twice the one of Fig. 7(d).

When rings expand, they suck the regulator V from the corona in front of the moving interface. The consequence of this process is that when two rings collide, they start to interact at a distance larger than the "hardcore" radius. This is shown in Fig. 8 which reproduces snapshots of two expanding
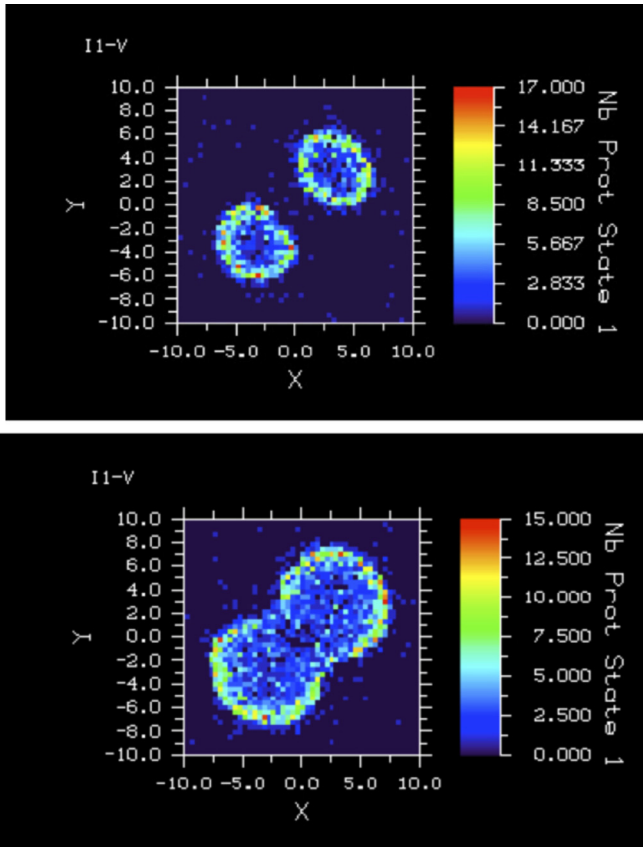
FIG. 8. Expanding rings. Case (a) corresponds to a snapshot for two expanding rings. For this set of parameters, the depletion-mediated interaction between the two rings distorts the circular shape of the rings which move away to optimize the diffusion of V. Case (b) corresponds to an annihilation dynamics where the two rings fuse in one (simulating box: 50×50).

rings in two generic cases. The top panel corresponds to the situation where the two rings first deform and repeal each other. The bottom panel corresponds to an annihilation dynamics where two expanding rings fuse together in one, so that small-scale features are also reproduced in the stochastic framework. In general, however, two expanding rings tend to avoid each other, cease from having a circular shape and repeal each other.

C. Clusters serve to digitize biochemical signals in the diffusion-uncoupled case

The model developed so far provides a simple mechanism for nucleation of IR clusters in the absence of cytoskeleton. When adhesion sites mature, local production of PIP$_2$ not only controls IR clustering but also controls actin dynamics to provide strong binding sites for IRs. Consequently, actin dynamics confiscate PIP$_2$ molecules and limit IR recruitment. In the usual case where adhesive complexes are much larger than the nascent adhesions studied so far, a simple model consists in limiting local production of PIP$_2$ with a finite density of ligands L distributed in an adhesive disk as in Fig. 9.
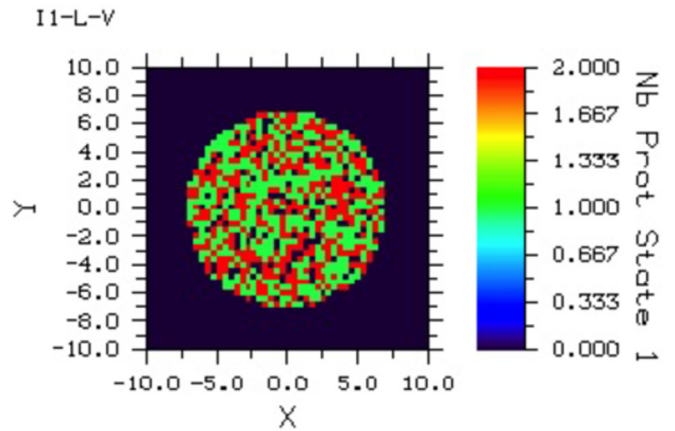

FIG. 9. Numerical simulations with an adhesive disk where receptors get immobilized by binding to ligands. The adhesive disk consists in a central disk with a finite number of ligands L per compartment, 2 in this case, and without any ligand outsidew. Only the complexes $I - L$ can bind V to trigger the feedback loop. This case corresponds to the diffusion-uncoupled regime where the diffusion of V is much faster than its association time so that the adhesive disk is homogeneously populated with dynamic clusters of active IRs.

Ligands immobilize active IRs as

$$I_a + L \underset{[l_-]}{\overset{[l_+]}{\rightleftharpoons}} I_a - L \tag{14}$$

with kinetic rates $l_\pm$. In what follows, only the species $I_a - L$ form with V a complex which produces U. When L is in very large excess, this intermediate step is irrelevant, since active IRs can always find available ligands. In parallel, the irreversible step Eq. (5) is now taken as

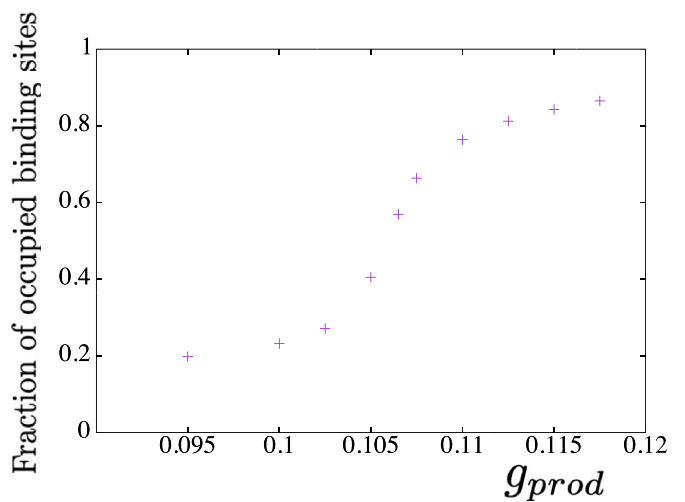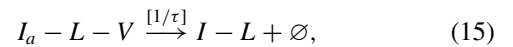$$I_a - L - V \overset{[1/\tau]}{\longrightarrow} I - L + \varnothing, \tag{15}$$

FIG. 10. Relative fraction of occupied ligand as a function of the feedback strength $1/\varepsilon$ in the adhesive disk of the pattern of Fig. 12. The system can be tuned from a low occupation probability to a high occupation probability by a small variation of the feedback strength (g_{prod}). This example corresponds to the system studied in the Appendices with one ligand molecule per compartment.

where τ is the dwell time of the complex $I - L - V$ producing the activator U. Equation (15) can be further generalized by adding another reaction step $I_a - L - V \xrightleftharpoons{[1/\tau]} I_a + L + \varnothing$ without change in the following.

To avoid spurious boundary effects where the activator is produced only at the rim of the adhesive disk, the diffusion of V and I must be much faster than the immobilization rate for binding I_a to L or V to $I - L$. This sets a maximum size of an adhesive disk controlled by the density L_0 of available ligands. In this diffusion-uncoupled regime, the adhesive disk is homogeneously populated by inactive receptors. The system can therefore take advantage of freely diffusive IRs to increase locally active receptors by a burst of activator.

As shown in Fig. 9, IR clusters are clearly observable at low enough rate of production g_{prod} where not all ligands are occupied. Increasing this rate drives the system to the fully occupied regime in a step wise manner; see Fig. 10. This is explained in Appendix D, where the system is shown to be analogous to a ϕ^3 theory with a threshold blurred by finite size effects. Membrane diffusive components can, therefore,

digitize signals by controlling the density of immobilization sites. Clearly, even in the low production rate regime, the feedback loop is enough to give small clusters of active IRs near the sites of production of u.

D. IR crosstalk

The same feedback mechanism can also be generalized to the case of a mixture of different families of IRs. A key regulator of this crosstalk is known to be the cytoskeleton binding proteins Talin which activates IRs [27,39] in a PIP$_2$ dependent way. Here, this crosstalk is studied by introducing two IR families, $I_{1,2}$, competing for immobilization sites with the production of the same activator U. As expected, a small molecular asymmetry between the two IRs is amplified by the feedback loop which localizes active receptors near the site of production of U.

A simple way to introduce this asymmetry is to take $\beta_2 > \beta_1$ for the off-rates $\omega_-(U)$ with equal affinities in Eqs. (14) and (15). In this case, the I_2 receptors spend more time in the active state and thus experience the slowest diffusive dynamics when they bind and unbind from the ligand.
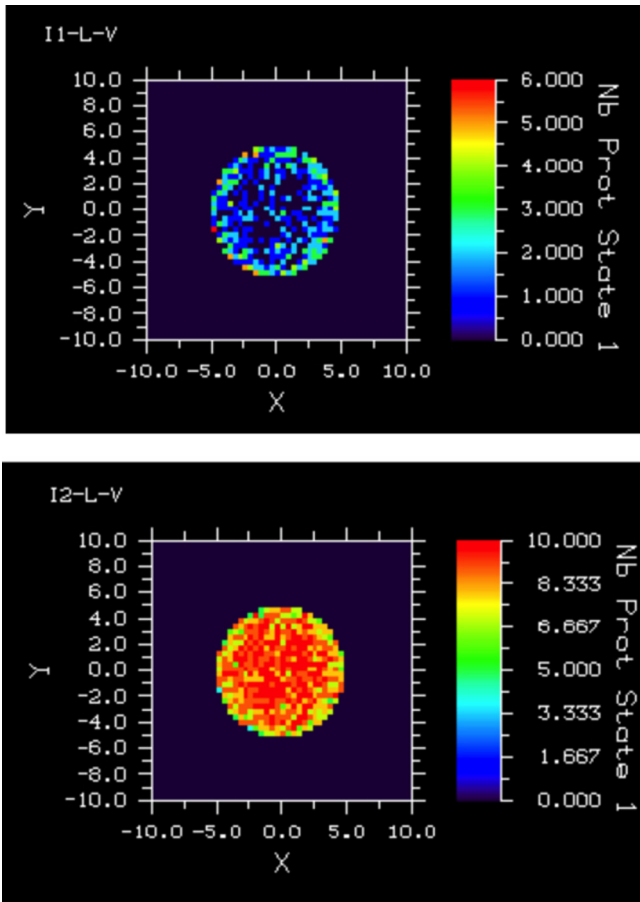

FIG. 11. A trans-regulation mechanism is a mechanism by which one receptor perturbs the binding of another receptors to a ligand. In this in example, two IRs, $I_{1,2}$, compete for the same ligand L. The two receptors have the same parameters but differ in their effective off-rates $\omega_-(u)$. Due to the feedback loop which increases the concentration of the receptor with the slowest dynamics, I_2, the binding of I_1 to L is down-regulated by I_2. 10 ligands per compartment.
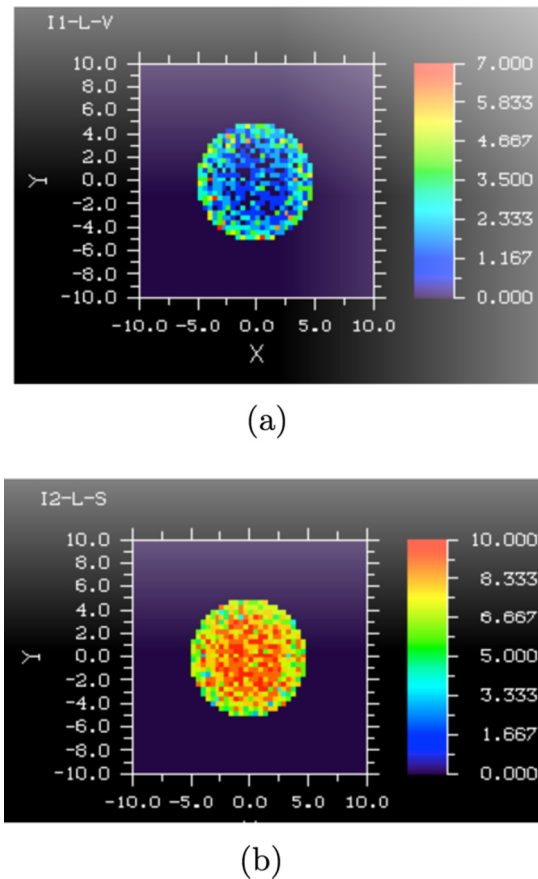
FIG. 12. Case where ligands are patterned inside the central adhesion disk, so that IRs can only bind ligands in this adhesive disk. The total number of ligands per compartment is 10 so that the central zone of disk is exclusively populated by type I_2 receptors with the longest dwell time $\tau_2 > \tau_1$ ($L = 10$)) for otherwise symmetric IRs. $K_{-,i} = 1/\tau_i$, $i = 1, 2$ for both integrin. The two kinases V and S are specific to $I_{1,2}$, respectively.

Because of the feedback, the relative concentration of active I_2 receptors is considerably increased in comparison to I_1's, and the probability for a ligand to bind an active I_2 is the highest. Ligands are thus dominantly bound to receptors of type 2.

This is the case in Fig. 11, where the two receptors have the same unperturbed densities to simulate the same expression level. Different scenarios can be considered depending on the effective off-rate $\omega_-(U)$ of the receptors. First, in the unmixed case and in the sufficiently large off-rate limit, $\omega_-(U)/\omega_+(U) < 1$ for the I_1 receptors, the fraction of occupied ligands approaches one while the fraction of unbound active IR is negligible. When I_1 receptors are now mixed with I_2 receptors with $\beta_2 = 2\beta_1$, the I_2 receptors switch off the I_1's by binding to the L's; see Fig. 11. As a result, mixing the two IR families drives the I_1's to the inactive state so that I_2 receptors down-regulate the signaling of I_1 which are now all inactive. In the other limit of not too large off-rate, the scenario is similar. The increase of I_2 due to the self-production of the activator still increases the density of the active receptors in the active state, so that the fraction of I_1 receptors bound to ligands is again negligible. However, because of the effective off-rate $\omega_-(U)$ of I_1, the fraction of active I_1 receptor is no more negligible so that they can bind other sites than L. In this case again, I_2 receptors regulate the binding of I_1 receptors to the ligands.

For simplicity, IR crosstalk has been analyzed in the simple scheme where the dynamics of the two receptors differ. Other mechanisms as kinase specificity or different binding times may also contribute to this crosstalk. For example, Fig. 12 demonstrates the same exclusion effect for two IR differing in their dwell times $\tau_{1,2}$ and when the kinases V and S are specific to the receptors. In general, the model predicts a trans-regulation mechanism which amplifies the concentration of IRs with the highest residence time near immobilization sites and which are therefore the most capable ones to transmit a mechanical force. Since actin polymerization and mechanical linkage are PIP_2 dependent and occur in concert, favoring the IRs with the highest residence time as predicted by the model gives a recruitment mechanism for the reinforcement of force transmission to the extracellular matrix.

IV. CONCLUSION

This paper combines conformational signaling with environment sensing to derive a model for IR clustering. Here this combination is implemented with a lifetime of a signaling receptor in its active state which depends on its membrane environment. The present approach departs from traditional Turing patterns usually described by classes of model with very different diffusivities and where the form of a polynomial nonlinearity determines the selection and the stabilization of patterns [40–42]. Here, these nonlinearities at the origin of IRs recruitment are fixed by a chemical potential for IR activation. Naturally, this chemical potential is modulated by the concentration of a key membrane phospholipid known to serve as a docking platform for numerous adhesive regulators. A point like excitation with a threshold gives nonequilibrium excited patterns with size corresponding to the diffusion length of this key membrane component. Clusters of receptors grow by lateral accretion and limiting factors resulting from the stress accumulation of IRs intercalating into rigid structures are neglected. This mechanism is validated in the stochastic regime and illustrates the role of robust parameters such as the size of the adhesive pattern and the ratio of the activator-regulator diffusion lengths.

To connect with cellular signaling, it may be helpful to recall that PIP_2 is easily transformed by many enzymatic activities. Its diffusion length is expected to be at most a few hundred of nanometers. Because this phopholipid controls many cellular processes including actin polymerization [17] and integrin activation, its local production at adhesive sites is well documented [15,43]. In particular, PIP_2 is produced at adhesive complexes by the PIKIγ kinase under the control of the kinase Src [18,20]. Src, additionally, is inactive in the cytosol and is recruited to the membrane where it diffuses to adhesive sites where it becomes active. For simplicity, the model presented in this paper lumps together these two kinases in one single module V and outlines these generic recruitment rules. PIP_2 can be considered as a fine regulator in the coordination of integrin since the specific ablation of PIPkIγ at adhesive impairs only temporally integrin activation [28] but has strong effects on integrin-cytoskeleton linkages and abolishes adhesion reinforcement. This is consistent with the present model where sites of PIP_2 production and sites of immobilization are spatially coordinated. Although other pathways working in synergy with PIP_2 signaling [44,45] are likely to occur, the feedback loop model of this paper predicts that active integrins should be coordinated and form nanoclusters as suggested in Ref. [23].

This work establishes also a formal casual relation between the dynamics of the IRs and their signaling properties, since dynamic receptors with relatively fast apparent diffusive motion can only form short-lived immobilized complexes. This principle could explain the different collective behaviors and patterning in adhesive complexes of two different IRs having slightly different binding properties. In particular, β_1 integrins, with slower dynamics in focal adhesive clusters than β_3 integrins, are spatially segregated from β_3 integrins in adhesive complexes [22] and podosome structures [24]. Integrin segregation in maturing adhesive complexes [46] and competition for binding talin has been invoked before as a trans-dominant inhibition between two integrin receptors [39]. This work links this phenomenon to PIP_2 local production and gives a differential recruitment mechanism for IRs which supports models for mechanical reinforcement as in Ref. [29].

As a final point, this paper together with Ref. [26], predicts that the type of localized excited adhesive structures strongly depends on the ratio of the two diffusion lengths for the activator and regulator. One way to change this ratio and to change IR patterning behavior is to engineer synthetic molecules which are directly recruited to adhesive sites. This approach has recently been taken in Ref. [47] where the use of photocontrolable SRC kinase demonstrates that IR clusters forming adhesive complexes reorganize into podosomes under the condition of direct SRC recruitment.

thank O. Destaing for his critical comments and his continuous inputs and encouragement.

APPENDIX A: SPIKE SOLUTIONS

Turing patterns are generically studied in reaction diffusion systems where species have very different diffusion constants and ratio of 100 are commonly reported in stochastic studies [36]. When the diffusion length of the inhibitor is much larger than the diffusion length of the activator, an asymptotic analysis for a simpler model is tractable in one dimension [48,49] and this analysis can only be partially extended to two-dimensional problems [50,51] for ring solutions. The method outlines below provides a simple analytical approach for the present 2D-model valid when the diffusion lengths are comparable in magnitude and it demonstrates how this model differs qualitatively from previous ones.

Assuming symmetry of revolution, it is convenient to rewrite Eqs. (1) as

$$
d_u \frac{1}{r} \frac{d}{dr} \left[r \frac{du}{dr} \right] - \frac{b}{\varepsilon} u = -\frac{1}{\varepsilon} v(r) n_a(u),
$$

$$
d_v \frac{1}{r} \frac{d}{dr} \left[r \frac{dv}{dr} \right] + \tilde{h}(v_h - v) = v \tilde{n}_a(u), \qquad (A1)
$$

where $\tilde{h}$ and $\tilde{n}_a(u)$ are defined as $\tilde{h} = h + n_a(u_h)$ and $\tilde{n}_a(u) = n_a(u) - n_a(u_h)$. Using this notation, the diffusion length $l_v = \sqrt{d_v/\tilde{h}}$ appears naturally, because $\tilde{n}_a(u)$ behaves as a Dirac δ function. We use fixed boundary conditions with $(u, v) = (u_h, v_h)$ so that $\tilde{n}_a(u)$ tends to zero as r goes to infinity with a spike centered at $r = 0$. In Eq. (A1), we assume also the IRs have converged to their asymptotic value, so that $n_a(u) = n_0 \omega_+^0 / \omega_-^0 e^{\beta u}$, $\beta = 1$.

These equations can be formally solved using the Green's function technique. Recall that if $w_0(z)$, $w_1(z)$ are two solutions of the homogeneous problem with boundary conditions $w_0'(z = 0) = w_1'(z = \infty) = 0$, then the Green's function with appropriate boundary conditions is

$$
G_x(z) = \frac{1}{x \mathscr{W}(x)} w_1(x) w_0(z) \quad \text{for } x \leqslant z,
$$

$$
G_x(z) = \frac{1}{x \mathscr{W}(x)} w_0(x) w_1(z) \quad \text{for } x \geqslant z, \qquad (A2)
$$

where $\mathscr{W}(x)$ is the wronskian.

For $d = 2$, $w_{0,1}(r)$ are Bessel's functions. Then $u(r)$ solves the integral equation

$$
u(r) = \frac{1}{d_u \varepsilon} \left[K_0(r/l_u) \int_0^r z dz \, I_0(z/l_u) v(z) n_a(u) + I_0(r/l_u) \int_r^\infty z dz \, K_0(z/l_u) v(z) n_a(u) \right], \quad (A3)
$$

where I_0, K_0 are Bessel functions of zero order. From Eq. (A1), $v(r)$ satisfies a similar equation. Specializing to $r = 0$, we have for the values of u and v at the maximum of
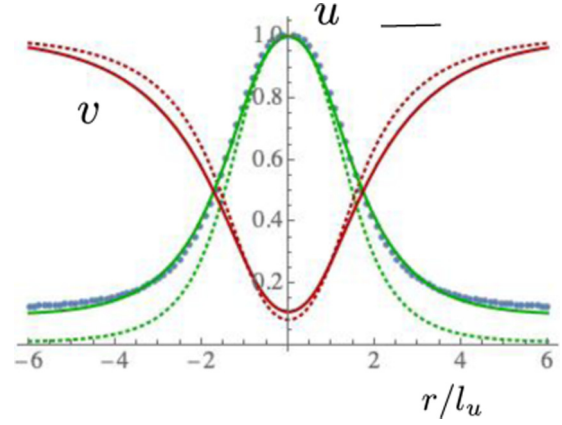

FIG. 13. Comparison between the analytical and numerical solutions for the spike solution along the boundary line of Fig. 4. The activator u and the regulator have equal diffusion constants, $d_u = d_v = 1$, with $l_v/l_u = 1.68$ as indicated by the bar. The continuous lines for $u(r)$ and $v(r)$ correspond to the numerical solutions of Eq. (1). The dotted lines for $u(r)$ and $v(r)$ are the analytical solutions corresponding to (u_s, v_s) solutions of Eq. (A7). Points on the continuous u-curve correspond to the analytical solution when Eq. (A5) is self-consistently calculated using $v(r)$ from the analytical solution. For convenience, u-curves have been normalized by their maximum values which almost coincides [$u_{\max} = 5.72$ for the direct integration and $u_{\max} = 5.92$ for system Eq. (A7)].

the spike

$$
u_s = \frac{1}{d_u \varepsilon} \int_0^\infty r dr \, K_0(r/l_u) v(r) \tilde{n}_a(u) + \frac{v_s}{v_h} u_h,
$$

$$
v_h - v_s = \frac{1}{d_v} \int_0^\infty z dz \, K_0(z/l_v) v(r) \tilde{n}_a(u), \qquad (A4)
$$

where

$$
\int_0^\infty r dr \, K_0(r/l_u) v(r) \approx v_s l_u^2, \qquad (A5)
$$

since $\tilde{n}_a(u) = n_a(u) + n_a(u_h)$ in the first equation with $n_a(u_h) \ll 1$. This is enough to calculate (u_s, v_s). For plotting $u(r)$ as in Fig 13, $u(r)$ must tend to u_h as $r \gg l_u$. When u_h is negligible, this does not pose problem, but to compare with numerical calculations at small but nonzero values of the activator in the quiescent state, one has to self-consistently evaluate this integral using $v(r)$ from the analytical solution for u to match u_h as r goes to infinity. As expected from Fig. 13, $v_h - v_s$ is well approximated by the 2D-Green's function $\propto -K_0(r/l_v)$.

Since $\tilde{n}_a(u)$ is strongly peaked at $r = 0$ and tends to zero at infinity, all integrals in Eq. (A4) can be evaluated using the saddle-point approximation. The second derivatives of u and v are known from the equations of motions. Equations (A4) are, therefore, equations for (u_s, v_s), and this system completely determines the solution. One finds for the second derivative

$$
u''(0) = \frac{1}{2 l_u^2} \left[u_s - \frac{1}{b} v_s n_a(u_s) \right],
$$

$$
v''(0) = \frac{1}{2 d_v} [v_s \tilde{n}_a(u_s) - \tilde{h}(v_h - v_s)], \qquad (A6)
$$

and all high order derivatives can be calculated in the same way.

Truncating this expansion to the second order gives only an approximation for the integrals but is enough to describe the bifurcation to the spike. One can now approximate $u(r)$ and $v(r)$ in Eq. (A4) and use definition Eq. (C1) of Appendix C to find

$$u_s = \frac{v_s \tilde{n}_a(u_s)}{b} F\left(\frac{w_s}{4}, l_u^2/d_v\right) + \frac{v_s}{v_h} u_h,$$

$$v_h - v_s = \frac{v_s \tilde{n}_a(u_s)}{\tilde{h}} F\left(\frac{l_v^2}{l_u^2}\frac{w_s}{4}, \frac{l_v^2}{l_u^2}\frac{l_u^2}{d_v}\right), \qquad \text{(A7)}$$

where $w_s = v_s \tilde{n}_a(u_s)/b - u_s$ is twice the magnitude of the curvature of u at $r = 0$ scaled by l_u^2 with definition Eq. (C3) for F.

To summarize, the saddle point approximation is a used as substitution method to replace the problem of finding a set of integral solutions by the problem of finding the solutions of an algebraic system. Once the values u_s and v_s are determined, the full solution can be obtained from Eq. (A3) using again the saddle point approximation. The main difference with the one-dimensional calculation [48,49] is that the curvature of $v(r)$ in not negligible in two dimensions even in the limit $l_v/l_u \gg 1$, so that $v(r)$ cannot be considered as constant within the spike.

APPENDIX B: RESULTS FOR THE SPIKE SOLUTION

In general, Eqs. (A7) can only be numerically solved. To proceed, the contour plots for the (u_s, v_s) solutions of these equations are plotted and the intersection points determined. Figure 14 demonstrates the generic behavior of these solutions as the ratio $d_v/(d_u\varepsilon)$ is varied. When this ratio is sufficiently large, the lateral diffusion of v is large enough to compensate for the loss of v within the spike. The system possesses two solutions at low and large values of the activator u_s in the spike. The small u_s solution approximates reasonably the numerical simulation, see Figs. 13 and 15, while the large u_s solution of Eq. (A7) is almost singular within the spike. This observation is consistent with a saddle-node bifurcation where a stable and unstable solutions merge together along the boundary line and cease to exist for lower ratio of $d_v/(d_u\varepsilon)$ when lateral diffusion is not strong enough. One interesting consequence of the saddle approximation is that the scaling of Eq. (A7) gives the geometry for the boundary line in Fig. 4 between the homogeneous state and the spike solution. Since the parameters ε and d_v enter only through the combination ε/d_v, the existence of solutions is only conditional to this ratio when both parameters are varied. As a result, the bifurcation between the homogeneous and the spike phases occurs along a line in the $(\varepsilon, d_v/d_u)$ plane for the phase diagram of Fig. 4.

To derive approximate asymptotic results, it is useful to approximate Eq. (A7) as

$$u_s = (u_s + w_s)F\left(w_s/4, l_u^2/d_v\right),$$

$$\frac{\tilde{h}v_h}{b} = (u_s + w_s)F\left(l_v^2 w_s/\left(4l_u^2\right), l_v^2/d_v\right), \qquad \text{(B1)}$$

since $v_s \ll v_h$ and to consider the asymptotic expansions derived in Appendix C. In practice, Eq. (B1) is a very good approximation to Eq. (A7).
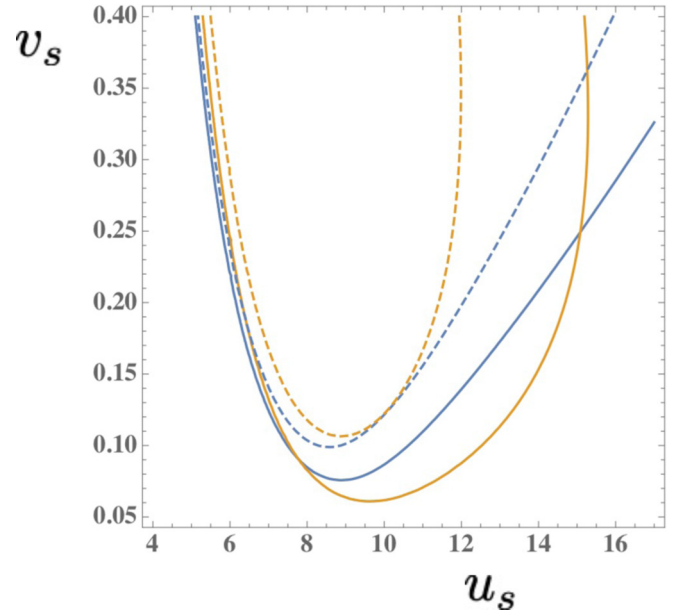

FIG. 14. Contour plot of the two self-consistent Eqs. (A7) in the (u_s, v_s) plane for different values of d_v/d_u. For sufficiently large values of d_v (continuous lines) the problem gives two intersection points at low and large values of u_s. The small u solution corresponds to case (a) of Fig. 15, while the large u solution has much stronger variations (not shown). Decreasing d_v ($\times 0.8$ for this case), the two solutions merge at a single point and ceases to exist below a threshold for $d_v/d_u\varepsilon$ (dashed lines) corresponding to the homogeneous-spike boundary line at the right of the phase digram of Fig. 4. Compared with the direct integration method of Fig. 4(a), this approach gives $(u_s, v_s) \approx (7.4, 0.1)$ instead of $(7.85, 0.16)$ from the direct numerical integration of the system.

Taking the ratio of the last two equations gives for u_s

$$u_s = \frac{\tilde{h}v_h}{b} \frac{F\left(w_s/4, l_u^2/d_v\right)}{F\left(l_v^2 w_s/\left(4l_u^2\right), l_v^2/d_v\right)}. \qquad \text{(B2)}$$

Ignoring logarithmic corrections of order $\ln(l_v^2/l_u^2)$, see Appendix C, one obtains a characteristic scale for the activator within the spike

$$u_s \approx \frac{l_v^2}{l_u^2} \frac{\tilde{h}v_h}{b} = \frac{d_v}{d_u} \frac{v_h}{\varepsilon}. \qquad \text{(B3)}$$

In practice, this expression overestimates the numerical result by a factor of order two, so that comparison with the numerical calculation is only possible by numerically solving Eq. (B1). This asymptotic expression gives, however, a lower bound for $d_v/(d_u\varepsilon)$ under which the spike solution ceases to exist. To derive it, it suffices to require that u_h must be larger than some threshold set by the natural rates of the IRs. One finds

$$\frac{d_v}{d_u} > \frac{\varepsilon}{v_h} \ln\left[\frac{\omega_-^0}{\omega_+^0}\right], \qquad \text{(B4)}$$

which overestimates the apparent slope of Fig. 4 by a factor 2 (where $v_h \approx 6.4$).

In conclusion, this method allows to identify characteristic orders of magnitude for the activator in the spike and for the
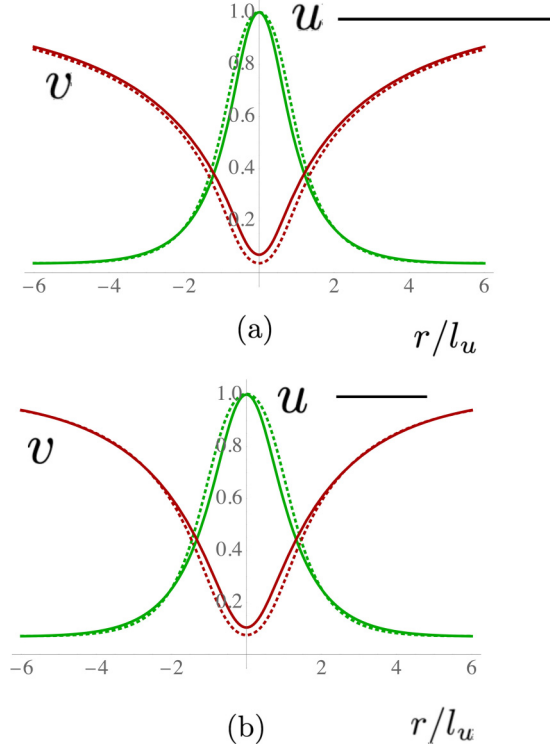
(a)

(b)

FIG. 15. Examples of spike solutions with symmetry of revolution for decreasing ratios of the diffusion lengths l_v/l_u indicated by the thick bar. From the top to the down, (a) $l_v/l_u = 5.26$, (b) $l_v/l_u = 2.80$. The continuous lines, with a maximum at the center of the spike, correspond to the activator u. The continuous lines, with a minimum, are plots of the regulator v. The dotted lines correspond to the saddle solutions for the same parameters. Cases (a) and (b) are for parameters on the boundary lines with the homogeneous phase; see Fig. 4. For graphical reasons, the plots of the activator u have been normalized by the same value $u(0)$, the saddle approximation Eq. (A7) giving the same result as the numerical solution within a few percent ($h = 0.02$, $b = 0.1$, $1/\varepsilon = 4.65$ for the top curve and $h = 0.05$, $b = 0.1$, and $1/\varepsilon = 2.6$ for the bottom one).

boundary line between the homogeneous and the spike phase of Fig. 4.

APPENDIX C: AN INTEGRAL

For what follows, it will be useful to consider the following integral, see Ref. [52], Eq. (6.63):

$$
\begin{aligned}
F_n(\alpha) &= \int_0^\infty x^n dx\, K_0(x) e^{-\alpha x^2} \\
&= \frac{1}{2\alpha^{n/2}} e^{\frac{1}{8\alpha}} \left[\Gamma\left(\frac{n+1}{2}\right) \right]^2 W_{-\frac{n}{2},0}\left(\frac{1}{4\alpha}\right).
\end{aligned} \tag{C1}
$$

When α is large, the following expansions hold:

$$
F_1(\alpha) \sim (\ln(4\alpha) - \gamma)/(4\alpha) + \dots,
$$
$$
F_3(\alpha) \sim (\ln(4\alpha) - \gamma - 1)/(4\alpha^2) + \dots, \tag{C2}
$$

where $\gamma = 0.577276\dots$ is the Euler constant.

As in Eq. (A7), one defines

$$
F(w, l_u^2/d_v) = F_1(w) + \frac{l_u^2}{4d_v v_s} [v_s \tilde{n}_a(u_s) - \tilde{h}(v_h - v_s)] F_3(w). \tag{C3}
$$

From the numerical point of view, $F_1(\alpha)/[\alpha F_3(\alpha)]$ approaches 1 only in the limit where $\ln(\alpha)$ is sufficiently large, so that strong logarithmic corrections to Eq. (B3) are expected.

APPENDIX D: CURRENT CONSERVATION AND ϕ^3 THEORY

This Appendix demonstrates the equivalence of the model with a ϕ^3 theory in the asymptotic limit where the activation of the feedback loop is simplified by introducing ligands for receptor immobilization. In the limit we consider, the limiting factor for the production of u is set by the number of ligands, so that we disregard the regulator V assuming that all $I - L$ complexes are bound to V. We introduce the molecular scheme

$$
I_a + L \underset{k_-}{\overset{k_+}{\rightleftharpoons}} I - L, \tag{D1}
$$

where an activated receptor binds an immobilized ligand to form a complex $I - L$. Conservation of ligands in each compartment implies the sum of complexed and free ligands must be constant, $L + I - L = L_0$. As in the text, we assume that ligands are patterned inside an adhesion disk of size R and that diffusion is sufficiently fast so that the concentration of bound receptors is homogeneously distributed inside the adhesive disk. We write $I_{a,\text{out}}$ or $I_{a,\text{in}}$ for the concentration of activated receptors outside and inside the adhesion disk. As before, the $I_{i,\dots}$'s correspond to inactive receptors.

Equilibrium between the active and inactive states of the receptors implies

$$
\omega_+(u) I_{i,\text{in}} - \omega_-(u) I_{a,\text{in}} = 0, \tag{D2}
$$

where u is the concentration of activator inside the disk. A similar relation holds outside the disk and

$$
I_{a,\text{out}} = \frac{\omega_+(0)}{\omega_-(0)} I_{i,\text{out}}, \tag{D3}
$$

with

$$
\frac{\omega_+(0)}{\omega_-(0)} \ll 1. \tag{D4}
$$

Finally, conservation of ligands implies that the number of complex $I - L$ scales as

$$
I - L = \frac{k_+ I_{a,\text{in}}}{k_+ I_{a,\text{in}} + k_-} L_0, \tag{D5}
$$

so that it suffices to know $I_{a,\text{in}}$ to know $I - L$.

To proceed, we note that current conservation for receptors at the boundary of the adhesive zone implies

$$
D_i I_{i,\text{out}} + D_a I_{a,\text{out}} = D_i I_{i,\text{in}} + D_a I_{a,\text{in}}, \tag{D6}
$$

where the $D_{i,a}$'s are diffusion constants for the active or inactive forms of receptors. We will take the limit $D_a \ll D_i$ as
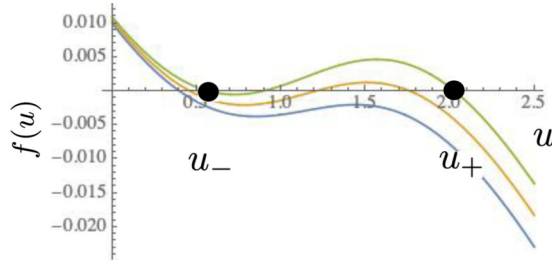
FIG. 16. Plot of the equivalent ϕ^3 functional $f(u)$ for $g_{\text{prod}} = 0.11$, 0.115, 0.12, where a is the rate of production of the activator as defined in Eq. (D11). For comparison with the stochastic simulations, the parameters are the same as the ones in Fig. 10. According to the Maxwell's condition, bifurcation takes place between the lowest u_- and highest u_+ root of $f(u)$ when the area under the curve is zero; see Eq. (D12). Note that the continuous limit gives a larger value for the feedback strength, i.e., ≈ 0.12, than its stochastic counterpart, i.e., ≈ 0.1075.

done in text. Outside the disk, the number of activated receptor is small so that $I_{a,\text{out}} = 0$. We conclude

$$I_{i,\text{in}} = I_{i,\text{out}} \left[1 + \frac{D_a}{D_i} \frac{\omega_+(0)}{\omega_-(0)} e^{\beta u} \right]^{-1}, \qquad (D7)$$

with

$$I_{a,\text{in}} = \frac{\omega_+(0)}{\omega_-(0)} e^{\beta u} I_{i,\text{in}}, \qquad (D8)$$

so that we can use Eq. (D5) to find $I - L$.

To simplify this expression, we assume the activated receptors have small diffusion constants, $D_i/D_a \ll 1$. In that case,

$$I - L = L_0 \left[1 + \frac{k_-}{k_+ I_{a,\text{in}}} \right]^{-1} = L_0 \left[1 + \frac{k_-}{k_+} \frac{\omega_-(0)}{\omega_+(0) I_{i,\text{in}}} e^{-\beta u} \right]^{-1}. \qquad (D9)$$

In the fast diffusive regime, $I_{i,\text{in}} = I_{i,\text{out}}$ is constant independent of u. Because $I - L$ is a function of u, we write $I - L = I - L(u)$ in Eq. (D9).

Assuming furthermore that the rate of production of u is proportional to $I - L$ with a proportionality constant g_{prod}, the equation of u takes the form

$$\frac{\partial u}{\partial t} = d_u \Delta u + f(u), \qquad (D10)$$

with

$$f(u) = -b_{\text{deg}} u + g_{\text{prod}} I - L(u), \qquad (D11)$$

where the irreversible degradation rate constant b_{deg} plays the same role as b/ε in the text. Plots of $f(u)$ are graphed in Fig. 16 and demonstrate that the rate of activation of u has the form of a single reaction diffusion with the property of bistability, since it admits two steady states given by the zeros $u_\pm$ of $f(u)$. Then, it is known that the stability criterion for switching from one solution to the other one is given by the Maxwell condition [34],

$$\int_{u_-}^{u_+} f(u) du = 0, \qquad (D12)$$

which can be meet by varying the rate of production g_{prod}. Comparison with the stochastic calculation of Fig. 10, see Fig. 16, demonstrates that the slight difference for the threshold value of a can be easily explained using finite sizes scaling arguments as in critical phenomena.

Finally, it is interesting to investigate the large off-rate limit

$$\frac{k_-}{k_+ I_{i,\text{in}}} \gg 1, \qquad (D13)$$

with a large number of ligands such that the ratio L_0/k_- stays finite. Then, by Eq. (D5) $I - L$ is finite and we neglect the changes in the concentration of ligands.

This means that the critical ratio for the effective functional in Eq. (D9),

$$\frac{k_-}{k_+ I_{i,in}} \frac{\omega_-(0)}{\omega_+(0)} e^{-\beta u} \gg 1, \qquad (D14)$$

is much larger than 1. In this limit, the equivalent Landau functional has an equivalent functional form of the one studied in the first part of this paper, or

$$-bu + a I_{i,in} \frac{k_+}{k_-} \frac{\omega_+(0)}{\omega_-(0)} e^{\beta u}. \qquad (D15)$$

[1] A. M. Turing, The chemical basis of morphogenesis, Philos. Trans. B Biol. Sci. **237**, 37 (1952).

[2] M. C. Cross and P. C. Hohenberg, Pattern formation outside of equilibrium, Rev. Mod. Phys. **65**, 851 (1993).

[3] A. J. Koch and H. Meinhardt, Biological pattern formation: From basic mechanisms to complex structures, Rev. Mod. Phys. **66**, 1481 (1994).

[4] S. Kondo and T. Miura, Reaction-diffusion model as a framework for understanding biological pattern formation, Science **329**, 1616 (2010).

[5] J. Halatek, F. Brauns, and E. Frey, Self-organization principles of intracellular pattern formation, Philos. Trans. R. Soc. Lond. B: Biol. Sci. **373**, 20170107 (2018).

[6] C. Albigès-Rizo, O. Destaing, B. Fourcade, E. Planus, and M. R. Block, Actin machinery and mechanosensitivity in invadopodia, podosomes, and focal adhesions, J. Cell. Sci. **122**, 3037 (2009).

[7] R. O. Hynes, Integrins: Bidirectional, allosteric signaling machines, Cell **110**, 673 (2002).

[8] R. Changede, X. Xu, F. Margadant, and M. P. Sheetz, Nascent integrin adhesions form on all matrix rigidities after integrin activation, Dev. Cell **35**, 614 (2015).

[9] M. J. Paszek, D. Boettiger, V. M. Weaver, and D. A. Hammer, Integrin clustering is driven by mechanical resistance from the glycocalyx and the substrate, PLoS Comput. Biol. **5**, e1000604 (2009).

[10] M. J. Paszek, C. C. DuFort, O. Rossier, R. Bainer, J. K. Mouw, K. Godula, J. E. Hudak, J. N. Lakins, A. C. Wijekoon, L. Cassereau, M. G. Rubashkin, M. J. Magbanua, K. S. Thorn, M. W. Davidson, H. S. Rugo, J. W. Park, D. A. Hammer, G. Giannone, C. R. Bertozzi, and V. M. Weaver, The cancer glycocalyx mechanically primes integrin-mediated growth and survival, Nature **511**, 319 (2014).

[11] E. Roob, III, N. Trendel, P. Rein ten Wolde, and A. Mugler, Cooperative clustering digitizes biochemical signaling and enhances its fidelity, Biophys. J. **110**, 1661 (2016).

[12] W. R. Holmes, B. Lin, A. Levchenko, and L. Edelstein-Keshet, Modelling cell polarization driven by synthetic spatially graded rac activation, PLoS Comput. Biol. **8**, e1002366 (2012).

[13] J. Das, M. Kardar, and A. K. Chakraborty, Positive feedback regulation results in spatial clustering and fast spreading of active signaling molecules on a cell membrane, J. Chem. Phys. **130**, 245102 (2009).

[14] M. Wehrens, P. R. ten Wolde, and A. Mugler, Positive feedback can lead to dynamic nanometer-scale clustering on cell membranes, J. Chem. Phys. **141**, 205102 (2014).

[15] G. Di Paolo and P. De Camilli, Phosphoinositides in cell regulation and membrane dynamics, Nature **443**, 651 (2006).

[16] J. Saarikangas, H. Zhao, and P. Lappalainen, Regulation of the actin cytoskeleton-plasma membrane interplay by phosphoinositides, Physiol. Rev. **90**, 259 (2010).

[17] P. A. Janmey, R. Bucki, and R. Radhakrishnan, Regulation of actin assembly by PI(4,5)P2 and other inositol phospholipids: An update on possible mechanisms, Biochem. Biophys. Res. Commun. **506**, 307 (2018).

[18] G. Di Paolo, L. Pellegrini, K. Letinic, G. Cestra, R. Zoncu, S. Voronov, S. Chang, J. Guo, M. R. Wenk, and P. De Camilli, Recruitment and regulation of phosphatidylinositol phosphate kinase type 1γ by the ferm domain of talin, Nature **420**, 85 (2002).

[19] V. Martel, C. Racaud-Sultan, S. Dupe, C. Marie, F. Paulhe, A. Galmiche, M. R. Block, and C. Albiges-Rizo, Conformation, localization, and integrin binding of talin depend on its interaction with phosphoinositides, J. Biol. Chem. **276**, 21217 (2001).

[20] K. Ling, R. L. Doughman, A. J. Firestone, M. W. Bunce, and R. A. Anderson, Type Iγ phosphatidylinositol phosphate kinase targets and regulates focal adhesions, Nature **420**, 89 (2002).

[21] F. Saltel, E. Mortier, V. P. Hytönen, M.-C. Jacquier, P. Zimmermann, V. Vogel, W. Liu, and B. Wehrle-Haller, New PI(4,5)P2- and membrane proximal integrin-binding motifs in the talin head control beta3-integrin clustering, J. Cell. Biol. **187**, 715 (2009).

[22] O. Rossier, V. Octeau, J.-B. Sibarita, C. Leduc, B. Tessier, D. Nair, V. Gatterdam, O. Destaing, C. Albigès-Rizo, R. Tampé, L. Cognet, D. Choquet, B. Lounis, and G. Giannone, Integrins β_1 and β_3 exhibit distinct dynamic nanoscale organizations inside focal adhesions, Nat. Cell. Biol. **14**, 1057 (2012).

[23] M. Spiess, P. Hernandez-Varas, A. Oddone, H. Olofsson, H. Blom, D. Waithe, J. G. Lock, M. Lakadamyali, and S. Strömblad, Active and inactive integrins segregate into distinct nanoclusters in focal adhesions, J. Cell Biol. **217**, 1929 (2018).

[24] O. Destaing, E. Planus, D. Bouvard, C. Oddou, C. Badowski, V. Bossy, A. Raducanu, B. Fourcade, C. Albiges-Rizo, and M. R. Block, β_1 integrin is a master regulator of invadosome organization and function, Mol. Biol. Cell. **21**, 4108 (2010).

[25] M. B. M. Meddens, E. Pandzic, J. A. Slotman, D. Guillet, B. Joosten, S. Mennens, L. M. Paardekooper, A. B. Houtsmuller, K. van den Dries, P. W. Wiseman, and A. Cambi, Actomyosin-dependent dynamic spatial patterns of cytoskeletal components drive mesoscale podosome organization, Nat. Commun. **7**, 13127 (2016).

[26] M. R. Block, O. Destaing, C. Petropoulos, E. Planus, C. Albigès-Rizo, and B. Fourcade, Integrin-mediated adhesion as self-sustained waves of enzymatic activation, Phys. Rev. E **92**, 042704 (2015).

[27] A. M. Gonzalez, R. Bhattacharya, G. W. deHart, and J. C. R. Jones, Transdominant regulation of integrin function: Mechanisms of crosstalk, Cell Signal **22**, 578 (2010).

[28] K. R. Legate, S. Takahashi, N. Bonakdar, B. Fabry, D. Boettiger, R. Zent, and R. Fässler, Integrin adhesion and force coupling are independently regulated by localized ptdins(4,5)(2) synthesis, EMBO J (2011).

[29] A. Elosegui-Artola, E. Bazellières, M. D. Allen, I. Andreu, R. Oria, R. Sunyer, J. J. Gomm, J. F. Marshall, J. L. Jones, X. Trepat, and P. Roca-Cusachs, Rigidity sensing and adaptation through regulation of integrin types, Nat. Mater. **13**, 631 (2014).

[30] A. Elosegui-Artola, R. Oria, Y. Chen, A. Kosmalska, C. Pérez-González, N. Castro, C. Zhu, X. Trepat, and P. Roca-Cusachs, Mechanical regulation of a molecular clutch defines force transmission and transduction in response to matrix rigidity, Nat. Cell. Biol. **18**, 540 (2016).

[31] See Supplemental Material at http://link.aps.org/supplemental/10.1103/PhysRevE.101.012420 for companion movies.

[32] J. Li and T. A. Springer, Integrin extension enables ultrasensitive regulation by cytoskeletal force, Proc. Natl. Acad. Sci. USA **114**, 4685 (2017).

[33] A. C. E. Shibata, T. K. Fujiwara, L. Chen, K. G. N. Suzuki, Y. Ishikawa, Y. L. Nemoto, Y. Miwa, Z. Kalay, R. Chadda, K. Naruse, and A. Kusumi, Archipelago architecture of the focal adhesion: Membrane molecules freely enter and exit from the focal adhesion zone, Cytoskeleton (Hoboken) **69**, 380 (2012).

[34] J. Murray, *Mathematical Biology* (Springer-Verlag, Berlin/Heidelberg, 1989).

[35] R. Erban, S. J. Chapman, and P. K. Maini, A practical guide to stochastic simulations of reaction-diffusion process, arXiv:0704.1908.

[36] Y. Cao and R. Erban, Stochastic Turing patterns: Analysis of compartment-based approaches, Bull. Math. Biol. **76**, 3051 (2014).

[37] M. Vigelius and B. Meyer, Stochastic simulations of pattern formation in excitable media, PLoS One **7**, e42508 (2012).

[38] C. B. Muratov, E. Vanden-Eijnden, and Weinan E, Self-induced stochastic resonance in excitable systems, Physica D **210**, 227 (2005).

[39] D. A. Calderwood, V. Tai, G. Di Paolo, P. De Camilli, and M. H. Ginsberg, Competition for talin results in trans-dominant inhibition of integrin activation, J. Biol. Chem. **279**, 28889 (2004).

[40] H. Meinhardt and A. Gierer, Pattern formation by local self-activation and lateral inhibition, Bioessays **22**, 753 (2000).

[41] M. Ward, Asymptotic methods for reaction-diffusion systems: Past and present, Bull. Math. Biol. **68**, 1151 (2006).

[42] J. Allard and A. Mogilner, Traveling waves in actin dynamics and cell motility, Curr. Opin. Cell Biol. **25**, 107 (2013).

[43] K. R. Legate and R. Fässler, Mechanisms that regulate adaptor binding to beta-integrin cytoplasmic tails, J. Cell. Sci. **122**, 187 (2009).

[44] J. Yang, L. Zhu, H. Zhang, J. Hirbawi, K. Fukuda, P. Dwivedi, J. Liu, T. Byzova, E. F. Plow, J. Wu, and J. Qin, Conformational activation of talin by riam triggers integrin-mediated cell adhesion, Nat. Commun. **5**, 5880 (2014).

[45] A. R. Gingras, F. Lagarrigue, M. N. Cuevas, A. J. Valadez, M. Zorovich, W. McLaughlin, M. A. Lopez-Ramirez, N. Seban, K. Ley, W. B. Kiosses, and M. H. Ginsberg, Rap1 binding and a lipid-dependent helix in talin F1 domain promote integrin activation in tandem, J. Cell. Biol. **218**, 1799 (2019).

[46] E. Zamir, M. Katz, Y. Posen, N. Erez, K. M. Yamada, B. Z. Katz, S. Lin, D. C. Lin, A. Bershadsky, Z. Kam, and B. Geiger, Dynamics and segregation of cell-matrix adhesions in cultured fibroblasts, Nat. Cell. Biol. **2**, 191 (2000).

[47] A. Kerjouan, C. Boyault, C. Oddou, E. Hiriart-Bryant, A. Grichine, A. Kraut, M. Pezet, M. Balland, E. Faurobert, I. Bonnet, Y. Coute, B. Fourcade, C. Albiges-Rizo, and O. Destaing, Molecular flux control encodes distinct cytoskeletal responses by specifying SRC signaling pathway usage, bioRxiv:10.1101/648030 (2019).

[48] C. B. Muratov and V. V. Osipov, Spike autosolitons in the Gray-Scott model, arXiv:patt-sol/9804001v4.

[49] C. B. Muratov and V. Osipov, Stability of the static spike autosilitons in the Gray-Scott model, SIAM J. Appl. Math. **62**, 1463 (2002).

[50] D. S. Morgan and T. J. Kaper, Axisymmetric ring solutions of the 2D Gray–Scott model and their destabilization into spots, Physica D **192**, 33 (2004).

[51] T. Kolokolnikov and J. Wei, On ring-like solutions for the gray-scott model: Existence, instability and self-replicating rings, Eur. J. Appl. Math. **16**, 201 (2005).

[52] I. Gradshteyn and I. Ryzhik, *Table of Integrals, Series, and Products* (Academic Press, San Diego, CA, 1980).